ChemComm

COMMUNICATION

View Article Online
View Journal | View Issue

Cite this: *Chem. Commun.*, 2018, **54**, 13123

Received 18th July 2018,
Accepted 29th October 2018

DOI: 10.1039/c8cc05860a

rsc.li/chemcomm

An evaporation induced self-assembly approach to prepare polymorphic carbon dot fluorescent nanoprobes for protein labelling†

Lei Li, Zhongyu Lian, Xi Yan, Meng Xia and Mingcui Zhang *

Herein, we report a novel route to prepare polymorphic carbon dot fluorescent probes *via* the evaporation-induced self-assembly of glutaraldehyde and carbon dots, which first usually form carbon nanoclusters which then could self-assemble to form carbon nanocrystals, nanospheres or nanofibers in different ionic strength solutions at room temperature. The aldehyde functionalized polymorphic C-dot fluorescent probe can easily covalently bond with amino groups on proteins.

The exploration and development of highly sensitive analytical methods for the detection of proteins, peptides, and other important biological molecules *in vivo* and in life is a hot and difficult topic in biomedical research. Therefore, biomarker technology is an indispensable research method in this field. The importance of efficient and sensitive fluorescent nanoprobes in biomedical research and practice has been rapidly increasing.[1,2] Many optical probes including organic dyes, semiconductor quantum dots, and upconversion nanoparticles have been widely used for biological labelling and imaging.[3–7] Most of these materials have unsatisfactory aspects. Organic dyes offer the advantages of high fluorescence quantum yields (QYs) and wide commercial availability. Unfortunately, organic dyes have poor photostability and solubility, which limit their further practical application in the field of chemical and biological analysis. To solve these problems, semiconductor quantum dots such as CdSe and CdTe have received increasing attention in recent decades owing to their highly tunable fluorescence properties and increased photostability. However, the flashing phenomenon of these traditional quantum dots still exists. Recently, rare earth dopant upconversion nanomaterials (UCNPs) that offer high photostability and thermal stability have received considerable attention for applications in sensing and bioimaging. Regrettably, synthesis of UCNPs is cumbersome.[8,9] Photobleaching and photoflashing may result in the degradation of the reliability of the measured results. Meanwhile, toxicity has greatly limited the application of these optical probes in the biomedical field.

Fluorescent carbon dots (C-dots) as a new class of fluorescent materials have demonstrated great potential for applications in direct imaging and biosensing,[10] disease diagnosis,[11] print ink,[12] photocatalysis,[13] and photovoltaic devices.[14] Compared to traditional fluorescent probes, the C-dots have their unique properties including significantly improved photostability, biological compatibility, drug delivery and green economy.[15–18] In particular, C-dots as a class of green labels have been used in bioanalysis, including immunoassays, western blots and immunohistochemistry, as they interact with specific biological molecules such as antibodies, peptides and adapters, coupled to increase the sensitivity of the assay.[19,20] However, the coupling reaction usually causes fluorescence quenching due to the aggregation of C-dots,[21–23] and thereby the sensitivity reduces. To overcome this shortcoming, researchers performed various functionalization reactions of C-dots. Min-Jung Kang designed silica nanospheres encapsulating a quantum dot-layer (SQS) to increase the quantum dot concentration and make them highly photoluminescent.[24] Aharon Gedanken used the C-dots embedded in a polyvinyl alcohol (PVA) polymer to prepare bright C-dots and improve the stability of the C-dots.[25] Dongxu Zhao prepared C-dot–NaCl hybrid crystals through a simple process to extend their light life.[26] Wei-Lung Tseng described a bottom-up assembly route for monodisperse C-dots into different sizes of C-dot aggregates through the control of the concentration of fatty acids provided in bright C-dots.[27] Nonetheless, the induce C-dot self-assembly method based on coupling agents to amplify marker signals for protein labelling is yet reported.

Recently, a new self-assembly method evaporation induced self-assembly (EISA) has attracted much attention. In this method, the molecules are introduced to the surface from solution, thus their conformation in the aqueous medium, which is mediated by intramolecular forces and surrounding intermolecular hydrogen bonds, can be significantly altered upon adsorption.[28] This self-assembly behaviour needs to be studied at the hydrophobic interface, however, most of them are based on silicon wafers.[29,30] When silicon is used as the carrier medium, edge enrichment is observed

Key Laboratory of Functional Molecular Solids, Ministry of Education, Key Laboratory of Chemo Biosensing, College of Chemistry and Materials Science, Anhui Normal University, Wuhu 241000, Anhui Province, China.
E-mail: zhangmc@mail.ahnu.edu.cn

† Electronic supplementary information (ESI) available: Experimental details and supplementary figures. See DOI: 10.1039/c8cc05860a

as a result of the interplay of contact line pinning, solvent evaporation and capillary flow.[31] Evidently, the preconcentration of this constituent cannot provide a decentralized reaction environment. However, the hydrophobic carbon film of this phenomenon has yet report. Inspired by this phenomenon, as a reference, we studied the self-assembly behavior of C-dots on hydrophobic carbon films based on glutaraldehyde-mediated C-dots. Compared to self-assembly in solution, these C-dots' self-assembly method does not need addition of a surfactant. Here we report a facile, safe and green synthesis of C-dot nanoclusters using glutaraldehyde coupled C-dots at room temperature. We chose glutaraldehyde for the following reasons. Firstly, hydroxylamine is formed directly from the aldehyde groups and amino groups in alkaline solutions without stringent conditions. Secondly, upon evaporation of the solvent, the products formed by the aldehyde groups and amino groups are greatly dehydrated and tend to be stable, which is beneficial for the self-assembly of C-dots. Most importantly, the C-dots self-assemble into a uniform monodisperse spherical structure in pH = 7.4 phosphate buffer and the aldehyde groups on the surface can further bind to the amino groups.[32] As a result, the evaporation-induced C-dot self-assembly gives rise to different morphologies under different ionic strength conditions. Crucially, the complex can further bind to the amino groups on the protein under approximately neutral conditions. This goes especially well with antibody labelling and bioanalytical conditions. This makes C-dots a powerful fluorescent labelling tool in the biomedical field.

In this study, we first demonstrate the formation of nanostructures with different morphologies on a carbon film, which was induced by evaporation, and then the C-dot nanoclusters were used for protein labelling. The C-dots were obtained through solvent-thermal treatment. After the hydrothermal reaction, a light yellow solution with blue emission under UV light was obtained, which indicates that the C-dots have been successfully prepared (Fig. S1, ESI†). Scheme 1 schematically depicts the entire process of the self-assembly of C-dots into polymorphic nanostructures under different conditions and drying through solvent evaporation. Basically, glutaraldehyde-mediated C-dot reactions generate C-dot nanoclusters at room temperature (Fig. S2, ESI†). Next, different concentrations of a sodium chloride or phosphate buffer solution were added to the carbon nanocluster solution, respectively, and then mixed uniformly. All samples were diluted 1000-fold on a copper grid and evaporated at room temperature. The carbon film on the copper network not only provides a good hydrophobic environment for evaporation-induced C-dot self-assembly, but more importantly, the morphology of the self-assembled C-dots formed on the carbon film can be observed using a transmission electron microscope (TEM) any time. Scheme 1 represents the carbon nanostructures formed under different conditions. Scheme 1a: the C-dot nanoclusters exhibit a monodispersed spherical structure in a pH = 7.4 (sodium hydroxide-adjusted PB solution) aqueous solution. Scheme 1b: maintaining pH = 7.4, the carbon nanoclusters exhibit a uniform linear structure when 0.1 M NaCl is added. Scheme 1c: maintaining pH = 7.4 and keeping 0.1 M NaCl constant, the carbon nanoclusters exhibit a nanobelt-shaped structure when 0.01 PBS is added. Scheme 1d: maintaining pH = 7.4, and keeping 0.1 M NaCl and 0.01 M PBS constant, the carbon nanoclusters exhibit a nanofiber morphology when 0.1 M PBS is added. The formation mechanism of glutaraldehyde, which mediates the self-assembly of single C-dot nanoparticles before solvent evaporation, is not clear yet. We propose the possible growth pathways: firstly, the aldehyde-functionalized single C-dots and the glutaraldehyde-mediated C-dot nanoclusters may exist simultaneously in the solution. Secondly, different ionic strengths and pHs have an important role in the nucleation process as the solvent evaporates.

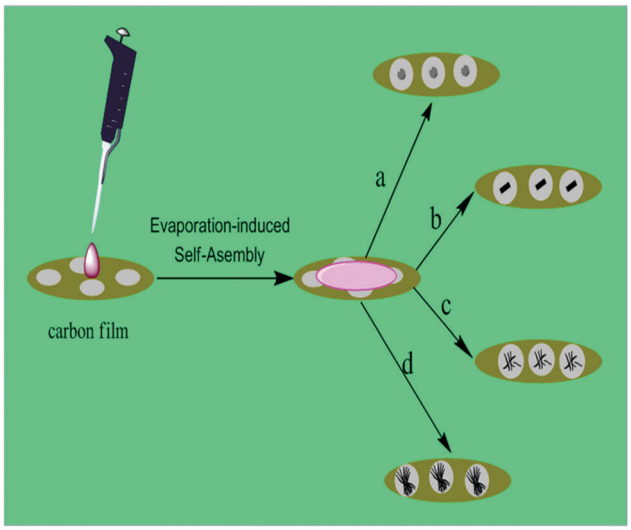

Scheme 1 Proposed mechanism for the self-assembly of C-dots nanostructure drying through solvent evaporation. a–d represent the C-dot nanostructures formed under conditions of pH = 7.4, 0.1 M NaCl, 0.01 M PBS and 0.1 M PBS, respectively.

The carbon nanoclusters aggregate to form a uniform sphere under approximately neutral conditions and show a clear morphology, which can be clearly seen from the embedded graph (Fig. 1a). The high-crystallinity carbon spheres are formed by evaporation-induced C-dot self-assembly under approximately neutral conditions. It is worth noting that there is a layer of an organic protective layer (red arrow in Fig. 1a) around these carbon spheres (blue arrow in Fig. 1a). This just confirms that the self-assembly of the C-dots into spherical structures induces self-assembly through solvent evaporation. This means the hydrogen bond is the most stable when the pH of the solution is under approximately neutral conditions.

When the solvent is left, the distance between the C-dots is pulled closer by the force of the hydrogen bond and they finally assembled into a highly crystalline carbon nanosphere. When the pH was changed from neutral to weakly acidic (pH = 6.0), the C-dot self-assembly morphology was still spherical but gradually blurred. Because the hydrogen bond is very unstable under acidic conditions, the final formation is loose self-assembled C-dots; and the other reason for the loose C-dots might be due to the pH responsiveness of the coupled C═N bonds[33] (Fig. S3, ESI†). The appearance of this phenomenon drove us to study the effect of ion intensity. We found that when 0.1 M NaCl was added to the reaction system and stirred overnight after mixing at 4 °C, the C-dots exhibited a carbon fiber morphology which could be seen by TEM imaging. As shown in Fig. 1b, the structure of the nanowire grows toward both ends

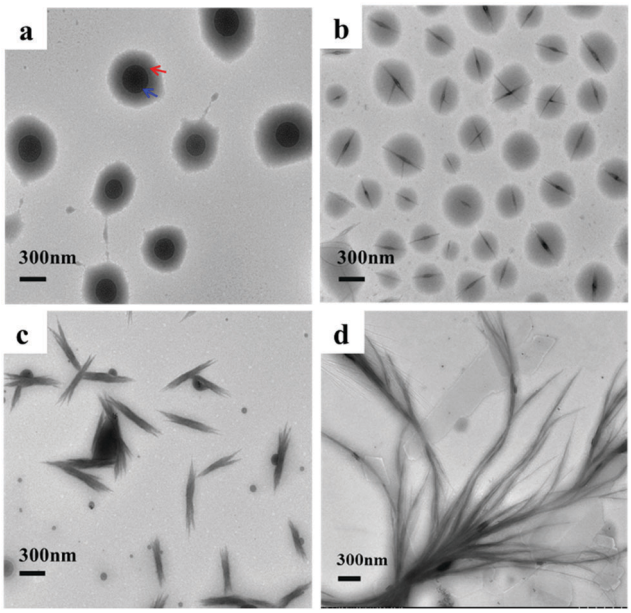

Fig. 1 TEM images obtained for the C-dot nanostructures dried from water solutions under different conditions: (a) pH = 7.4, (b) 0.1 M NaCl, (c) 0.01 M PBS, and (d) 0.1 M PBS, respectively.

centered on the nanoclusters in the evaporated area. The possible reason is the electrostatic interaction between the sodium ions and the carbon nanoclusters, which increased the density of the carbon atoms. Finally, this increases the assembling efficiency and stability.[34] Fortunately, as the solvent is reduced, the C-dot nanoclusters cluster into nanowires at high concentrations of sodium chloride solution. The traces left by the solvent around the nanowires can be clearly seen in the TEM image. At the same time, we continued to explore the impact of phosphate buffer under the same processing conditions. The results correspond to previous ideas. As shown in Fig. 1c, the C-dot nanoclusters self-assemble into obvious nanoribbons in 0.01 M phosphate buffer. From the two ends of the nanoribbon, it can be clearly seen that this nanoribbon is formed by the accumulation of many nanofibers. Next, we studied the influence of increase of the concentration of phosphate buffer, for which we treated the C-dot nanoclusters with 0.1 M phosphate buffer. It can be seen from Fig. 1d that the C-dot nanofibers became bigger in size and both ends were in a divergent state when the concentration of the phosphate buffer solution was increased. Compared to the sodium chloride buffer solution, the C-dot nanofibers formed in the phosphate buffer with no obvious solvent around it. Therefore, phosphate buffer plays a major role in the formation of C-dot nanofibers compared to sodium chloride solutions. Because phosphate is a cross-shaped needle crystal, it can be attached as a C-dot nanocluster to form large-sized C-dot nanofibers (Fig. S4, ESI†).

To confirm the components of the multi-morphological self-assembled C-dots, they were characterized by Raman spectroscopy, energy dispersive X-ray (EDX) spectroscopy, dynamic light scattering (DLS) and X-ray photoelectron spectroscopy (XPS). Raman spectra of the original C-dots are shown in Fig. 2a. The peaks centered at *ca.* 1343 and 1540 cm^{-1} are attributed to the D (disordered sp^3-hybridized carbon) and G (ordered sp^2-hybridized carbon) bands, respectively, of the carbon materials. Raman spectra of the self-assembly of the C-dots under conditions of pH (b), NaCl (c), 0.01 M PBS (d) and 0.1 M PBS (e) are included in Fig. 2 for comparison. It was observed that all of these self-assembly of the C-dots under conditions of pH, NaCl, 0.01 M PBS and 0.1 M PBS contain D and G bands, respectively. The energy dispersive X-ray (EDX) spectrum also shows different self-assembly conditions with composition of elements (Fig. S5, ESI†). On the other hand, the C-dots only show the signals of C, N and O (Fig. S5, ESI†). The size distribution of the C-dots and the multi-morphological self-assembled C-dots are shown in Fig. S6, ESI.† The multi-morphological self-assembled C-dots were further confirmed by X-ray photoelectron spectroscopy (XPS) (Fig. S7, ESI†). All means of characterization proved that the observed nanostructure was actually a C-dot-assembly instead of a residual salt in the C-dot solution after evaporation.

Of particular interest to us is when proteins are added to the pre-prepared C-dot nanoclusters, the C-dot protein complexes are further formed, meanwhile the proteins are labelled. This provides a rapid labelling method for proteins at room temperature. In this experiment, we chose to use antibodies (antibody titer is 1 : 64 000, Fig. S8, ESI†) as the research object, because we can prove whether or not it is labelled by the specific reaction of antigen antibodies. Before validation, we performed FTIR spectroscopy (Fig. S9, ESI†) and TEM imaging of the C-dot antibody complexes, respectively. The TEM images of the C-dots, carbon nanoclusters, and C-dot antibody complexes can be clearly seen in Fig. 3. Fig. 3a indicates good dispersibility of the C-dots with slight random agglomerations. Upon adding glutaraldehyde under stirring at room temperature, the C-dots assemble to form larger C-dot nanoclusters (Fig. 3b). The C-dot nanocluster labelled antibody form composite was also demonstrated by TEM images. As shown in Fig. 3c, the C-dot nanoclusters and antibodies are coupled by glutaraldehyde to form uniformly dispersed nanospheres. Finally, C-dot antibody complexes formed when the antibodies were added. More importantly, from the inset of the TEM image shown in Fig. 3c, we can clearly see the formation of a layer of protein corona on the surface of a C-dot nanocluster. This is a better demonstration of the successful labelling of the antibody with

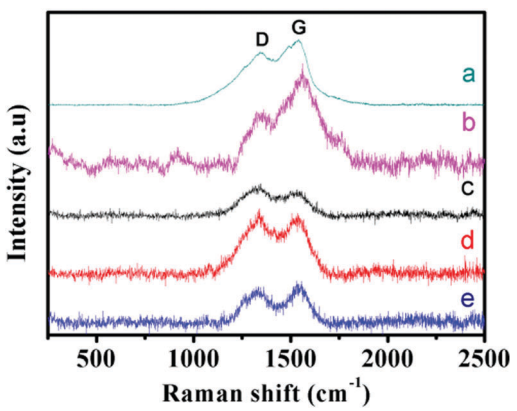

Fig. 2 Raman spectra of the original C-dots (a), the self-assembly of C-dots under conditions of pH = 7.4 (b), 0.1 M NaCl (c), 0.01 M PBS (d) and 0.1 M PBS (e), respectively.

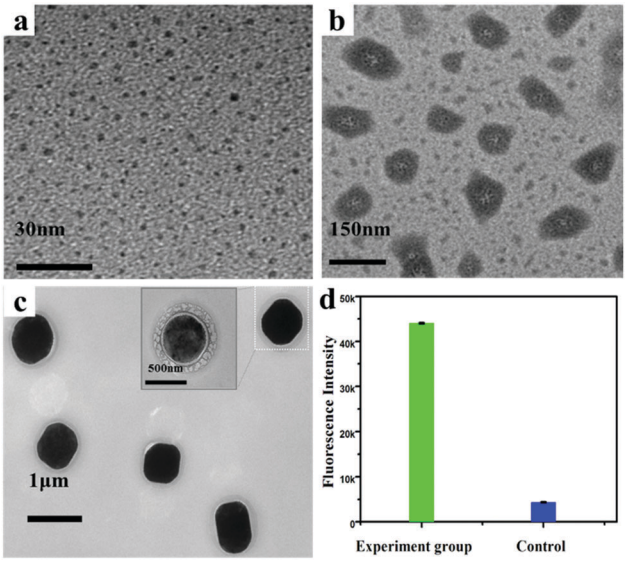

Fig. 3 TEM image of the C-dots (a), C-dot nanoclusters (b), carbon nanoclusters and antibody composite (c). Fluorescence intensity value of the C-dot–antibody complex and the untreated antibody to detect the antigen (d).

the C-dot nanoclusters, and the optimized adsorption capacity of the antibody is 2.5 mg mL^{-1} (Fig. S10, ESI†). Further, we performed a direct fluorescent immunoassay to demonstrate the utility of the fluorescent probe, where the experiment group fluorescence intensity was noticeably raised about 44 025 as shown in Fig. 3d (green column), which is about 10 times that of the blank control group. By contrast, when only C-dots were examined, no significant fluorescence signal was observed (Fig. 3d, blue column), indicating the good specificity and selectivity of the proposed fluorescent immunoassay. Thus, these comparison results indicate adequately that the prepared probes *via* C-dots labelled anti-nano-drug deliver antibody could be used to sensitively detect nano-drug deliver through the amplification of signals. At the same time, the ultraviolet absorption spectrum also provides a good proof (Fig. S11, ESI†).

In summary, combined with evaporation-induced self-assembly techniques, green non-toxic C-dots and glutaraldehyde coupling agents, we first studied the morphology of C-dot nanostructures by solvent evaporation on carbon films. Then, the C-dot nanoclusters further formed complexes with the protein at room temperature. We further verified the fluorescence intensity of the C-dot antibody complex by a fluorescence immunoassay, which is about 10 times that of the blank control group. As can be observed from these preliminary results, glutaraldehyde-mediated carbon nanoclusters are not only intermediates for the formation of multi-modal nanomaterials, but more importantly, they can also form complexes with proteins. This will have a very beneficial impact on the field of biomarkers.

The authors gratefully acknowledge the financial support from the National Natural Science Foundation of China (No. 21175004).

Conflicts of interest

There are no conflicts to declare.

Notes and references

1 G. F. Zheng, X. P. A. Gao and C. M. Lieber, *Nano Lett.*, 2010, **10**, 3179–3183.
2 S. Y. Xu, X. L. Bai, J. W. Ma, M. M. Xu, G. F. Hu, T. D. James and L. Y. Wang, *Anal. Chem.*, 2016, **88**, 7853–7857.
3 K. Lee, S. Mandal, J. Morry, O. Srivannavit, E. Gulari and J. Kim, *Chem. Commun.*, 2013, **49**, 4528–4530.
4 U. Resch-Genger, M. Grabolle, S. Cavaliere-Jaricot, R. Nitschke and T. Nann, *Nat. Methods*, 2008, **5**, 763–775.
5 I. L. Medintz, H. T. Uyeda, E. R. Goldman and H. Mattoussi, *Nat. Mater.*, 2005, **4**, 435–446.
6 A. Xia, Y. Gao, J. Zhou, C. Y. Li, T. S. Yang, D. M. Wu, L. M. Wu and F. Y. Li, *Biomaterials*, 2011, **32**, 7200–7208.
7 J. K. Wang, N. He, Y. L. Zhu, Z. B. An, P. Chen, C. A. Grimes, Z. Nie and Q. Y. Cai, *Chem. Commun.*, 2018, **54**, 591–594.
8 S. J. Liu, L. L. Zhang, T. S. Yang, H. R. Yang, K. Y. Zhang, X. Zhao, W. Lv, Q. Yu, X. L. Zhang, Q. Zhao, X. M. Liu and W. Huang, *ACS Appl. Mater. Interfaces*, 2014, **6**, 11013–11017.
9 X. Xie, N. Gao, R. Deng, Q. Sun, Q. H. Xu and X. Liu, *J. Am. Chem. Soc.*, 2013, **135**, 12608–12611.
10 J. Wen, Y. Q. Xu, H. J. Li, A. P. Lu and S. G. Sun, *Chem. Commun.*, 2015, **51**, 11346–11358.
11 E. J. Goh, K. S. Kim, Y. R. Kim, H. S. Jung, S. Beack, W. H. Kong, G. Scarcelli, S. H. Yun and S. K. Hahn, *Biomacromolecules*, 2012, **13**, 2554–2561.
12 Q. H. Liang, W. J. Ma, Y. Shi, Z. Li and X. M. Yang, *Carbon*, 2013, **60**, 421–428.
13 X. Han, Y. Z. Han, H. Huang, H. C. Zhang, X. Zhang, R. H. Liu, Y. Liu and Z. H. Kang, *Dalton Trans.*, 2013, **42**, 10380–10383.
14 C. Xie, B. Nie, L. H. Zeng, F. X. Liang, M. Z. Wang, L. B. Luo, M. Feng, Y. Q. Yu, C. Y. Wu, Y. C. Wu and S. H. Yu, *ACS Nano*, 2014, **8**, 4015–4022.
15 H. T. Li, Z. H. Kang, Y. Liu and S. T. Lee, *J. Mater. Chem.*, 2012, **22**, 24230–24253.
16 Q. Li, T. Y. Ohulchanskyy, R. L. Liu, K. Koynov, D. Q. Wu, A. Best, R. Kumar, A. Bonoiu and P. N. Prasad, *J. Phys. Chem. C*, 2010, **114**, 12062–12068.
17 X. H. Zhu, T. B. Zhao, Z. Nie, Y. Liu and S. Z. Yao, *Anal. Chem.*, 2015, **87**, 8524–8530.
18 M. A. Cohen and M. P. Vandenbergh, *Energy Economics*, 2012, **34**, S53–S63.
19 M. Zhou, E. Nakatani, L. S. Gronenberg, T. Tokimoto, M. J. Wirth, V. J. Hruby, A. Roberts, R. M. Lynch and I. Ghosh, *Bioconjugate Chem.*, 2007, **18**, 323–332.
20 L. Zhu, G. H. Xu, Q. Song, T. Tang, X. Wang, F. D. Wei and Q. Hu, *Sens. Actuators, B*, 2016, **231**, 506–512.
21 Y. Ooyama, S. Yoshikawa, S. Watanabe and K. Yoshida, *Org. Biomol. Chem.*, 2006, **4**, 3406–3409.
22 C. L. Chiang, M. T. Wu, D. C. Dai, Y. S. Wen, J. K. Wang and C. T. Chen, *Adv. Funct. Mater.*, 2005, **15**, 231–238.
23 B. Kong, J. Tang, Y. Y. Zhang, T. Jiang, X. G. Gong, C. X. Peng, J. Wei, J. P. Yang, Y. C. Wang, X. B. Wang, G. F. Zheng, C. Selomulya and D. Y. Zhao, *Nat. Chem.*, 2016, **8**, 171–178.
24 H. Han, J. C. Pyun, H. Yoo, H. S. Seo, B. H. Jung, Y. S. Yoo, K. Woo and M. J. Kang, *Anal. Chem.*, 2014, **86**, 10157–10163.
25 V. B. Kumar, A. K. Sahu, A. M. Mohsin, X. P. Li and A. Gedanken, *ACS Appl. Mater. Interfaces*, 2017, **9**, 28930–28938.
26 H. Z. Liu, F. Wang, Y. P. Wang, J. J. Mei and D. X. Zhao, *ACS Appl. Mater. Interfaces*, 2017, **9**, 18248–18253.
27 T. H. Chen and W. L. Tseng, *Anal. Chem.*, 2017, **89**, 11348–11356.
28 D. Li, Z. W. Zhou, J. Qin, Y. Li, Z. R. Liu and W. L. Wu, *ChemistrySelect*, 2018, **3**, 2479–2486.
29 A. Mazloomi Moqaddam, D. Derome and J. Carmeliet, *Langmuir*, 2018, **34**, 5635–5645.
30 Z. C. Feng, *Microelectron. Eng.*, 2006, **83**, 165–169.
31 R. D. Deegan, O. Bakajin, T. F. Dupont, G. Huber, S. R. Nagel and T. A. Witten, *Nature*, 1997, **389**, 827–829.
32 I. Migneault, C. Dartiguenave, M. J. Bertrand and K. C. Waldron, *Biotechniques*, 2004, **37**, 790–796.
33 C. Xu, X. Guan, L. Lin, Q. Wang, B. Gao, S. Zhang, Y. Li and H. Tian, *ACS Biomater. Sci. Eng.*, 2017, **4**, 193–199.
34 J. Kwon, M. Lee and S. Na, *J. Comput. Chem.*, 2016, **37**, 1839–1846.

